The effect of prior austenite grain size on hydrogen embrittlement of Co-containing 18Ni 300 maraging steel

Article *in* International Journal of Hydrogen Energy · June 2019

DOI: 10.1016/j.ijhydene.2019.05.074

CITATIONS
18

READS
28

7 authors, including:

Jorge Luiz Cardoso
Universidade Federal do Ceará
12 PUBLICATIONS **39** CITATIONS
SEE PROFILE

Luis Paulo Santos
Universidade Federal do Ceará
16 PUBLICATIONS **140** CITATIONS
SEE PROFILE

Juan Manuel Pardal
Universidade Federal Fluminense
120 PUBLICATIONS **1,648** CITATIONS
SEE PROFILE

Available online at www.sciencedirect.com

ScienceDirect

journal homepage: www.elsevier.com/locate/he

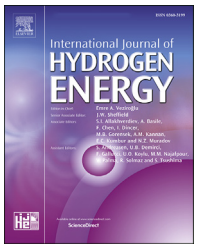

The effect of prior austenite grain size on hydrogen embrittlement of Co-containing 18Ni 300 maraging steel

Marcelo J. Gomes da Silva [a,*], *Jorge L. Cardoso* [a], *Dayane S. Carvalho* [a], *Luis P.M. Santos* [b], *Luís Flávio G. Herculano* [a], *Hamilton F. Gomes de Abreu* [a], *Juan M. Pardal* [c]

[a] *Universidade Federal do Ceará, Departamento de Engenharia Metalúrgica e de Materiais, Campus do Pici, Bloco 729/730, CEP 60445-554, Fortaleza, CE, Brazil*

[b] *Universidade Federal do Ceará, Programa de Pós-graduação em Química, Campus do Pici, Bloco 939/940, CEP 60400-900, Fortaleza, CE, Brazil*

[c] *Universidade Federal Fluminense, Departamento de Engenharia Mecânica, Campus da Praia Vermelha, Rua Passo da Pátria, CEP 24210-240 Niterói, RJ, Brazil*

ARTICLE INFO

Article history:
Received 14 March 2019
Received in revised form
23 April 2019
Accepted 11 May 2019
Available online 1 June 2019

Keywords:
Maraging steel
Hydrogen embrittlement
Prior austenite
Grain sizes
Hydrogen-induced cracking

ABSTRACT

The effects of the prior austenite grain sizes in hydrogen embrittlement of Co-containing 18Ni 300 maraging steel were studied employing Slow Strain Rate Testing (SSRT) in 0.6 M NaCl electrolyte under simultaneuos cathodic polarization. The material was susceptible to hydrogen embrittlement in all investigated conditions. In addition, the examination of the fractured surface revealed that the presence of hydrogen in steel promotes the formation of quasi-cleavage regions and hydrogen-induced cracks along the grain boundaries. However, the refining of the prior austenite grain allowed an improvement in the HE resistance. Moreover, EBSD analysis showed that intergranular cracks propagated along to grain boundaries orientated to {001} planes parallel to normal direction, whereas they were deflected on {101} and {111} crystallographic planes.

Introduction

The 18Ni maraging steels are a special class of materials, which present a combination of high-strength and high toughness. These mechanical properties have made 18Ni maraging steels widely used in critical applications, such as aeronautic and military industries [1]. These high-strength steels are characterized by a low carbon content and are hardened by the precipitation reactions of fine intermetallic compounds during the aging treatment [2]. Typically, the combination of Co and Mo alloying elements leads to an effective hardening in 18Ni maraging steels [2,3]. In general, the heat treatment employed in alloys involves the solution annealing at elevated temperatures above 800 °C and then cooling to room temperature, which leads the formation of the

* *Corresponding author.*
E-mail address: mgsilva@ufc.br (M.J. Gomes da Silva).
https://doi.org/10.1016/j.ijhydene.2019.05.074

well-known soft body martensite phase [1–3]. Finally, the material is submitted to an aging treatment at temperature ranging between 400 and 640 °C that promotes the precipitation of nano-sized intermetallic phases, such as Ni_3(Ti,Mo), Ni_3Ti, μ-phase and Fe_2Mo in the martensitic matrix, which are responsible for the excellent mechanical properties of these materials [1,4–8]. In addition, aging above 500 °C leads the reversion of austenite from the partially decomposition reaction of martensite by diffusion-controlled mechanism [6,9]. The presence of reverted austenite in 18Ni maraging steels has serious implications on their mechanical and magnetic properties [10–12].

It is known that the ultra-high strength 18Ni maraging steels can undergo environmentally assisted cracking, such as hydrogen embrittlement (HE) when exposed to hydrogen-rich environment [13–21]. In case of the Co-free 18Ni maraging steels several works considering the topic can be found in the literature [13–18]. Rao et al. [13], studied the effect of stress concentration factor in 18Ni 2400 (T-350) maraging steel aged at 510 °C for 1 h in synthetic seawater environment. These authors observed a drastically reduction in notched tensile strength and time to fracture of steel after testing, as well as, intercrystalline fracture mode on crack region. In addition, hydrogen assisted cracking of T-250 maraging steel aged at 480 °C for 2 h has been reported in air when the relative humidity (RH) was ≥30% [15]. Moreover, Tsay et al. [17], demonstrated that T-200 maraging steels aged at 427 °C, 482 °C and 538 °C were susceptible to HE in the saturated H_2S solution. On the other hand, considering the Co-containing 18Ni maraging steel a significant amount of studies dedicated to understand this phenomenon are also found [19–24]. In the 1970s Wei and co-works [19–21] revealed that different grades of 18Ni maraging steels exhibited similar crack growth kinetics under gaseous hydrogen atmosphere. Reddy et al. [22], reported that tensile properties and fracture characteristics of 18Ni 250 maraging steel have been correlated with the quantity of hydrogen picked up by the steel, additionally, they observed a change in fracture surface from ductile dimples to mixed mode, intergranular separation and transgranular cleavage as the amount of absorbed hydrogen increased. However, few works are devoted to investigate HE in grade 300 18Ni maraging steel. Santos et al. [23], studied HE of ultra-high strength 18Ni 300 maraging steel and observed that the intergranular cracks propagate mainly along grain boundaries with {001}//ND fiber orientation. Besides, Béreš and collaborators [24] employing *in situ* synchrotron X-ray diffractionin this material to revealed that the {001} parallel to normal direction (ND) are cystallographic planes on which undergo highest magnitude of lattice strain during tensile loading, further this study showed that the cracks were arrested when faced {111}//ND.

Currently, several studies have been conducted to investigate the role of microstructure into the HE of ultra-high strength steels [25–31], such as austenitic stainless steel [32], dual-phase (DP), quenched and partitioned (Q&P), and twinning induced plasticity (TWIP) steels [33], 17-4 PH stainless [34], low-alloy steels [35] and 18Ni maraging steels [14,16,17,36]. Wang et al. [36], claimed that in over-aged condition Co-containing TM210 maraging steel exhibited higher resistance to HE, additionally, they also observed that HE susceptibility depends on reverted austenite content. In addition, it has been already reported that reverted austenite acts as irreversible hydrogen traps in maraging steels, which prevents the transport of hydrogen inward to the highly strained region [16,17]. Furthermore, Tsay et al. [14], demonstrated that in the coarse-grained structure would raise the HE susceptibility of T-200 maraging steel and also the fracture features.

Therefore, the aim of this work was to evaluate the influence of grain size in the HE of the 18Ni 300 maraging steel. In order to obtain samples with different grain size the material was solution annealed at four temperatures combined with two aging conditions. In addition slow strain rate tests (SSRT) were carried out in air and under hydrogen environment. Finally, electron backscattering diffraction (EBSD) was performed on fractured surface.

Material and experimental

Material

The material used in this research was the commercial Co-containing 18Ni 300 maraging steel. The chemical composition of this alloy in weight percent is 18.28 Ni, 9.41 Co, 4.73 Mo, 0.73 Ti, balance Fe.

Heat treatments and XRD characterization

In order to obtain samples with different grain sizes, the solution annealing treatment of the 18Ni 300 maraging steel (1.5 cm × 1.0 cm × 1.5 mm) was performed at 840 °C, 950 °C, 1050 °C and 1150 °C in a muffle furnace during a period of 1 h followed by an air cooled to room temperature and then divided in two groups of samples. The first group of samples was aged at 480 °C for 3 h and the second oneat 560 °C for 1 h. After aging, the samples were air cooled.

X-ray diffraction (XRD) measurements were also carried out on the samples aged at 560 °C for 1 h in order to detect any reverted austenite. The samples were sanded up to 400 mesh (SiC paper). The measurements were carried out using a Philips® X'Pert Pro diffractometer with a radiation of CoKα (0.1789 nm). The 2θ angle ranged from 45° to 104°. This measurement was carried out only for the second group of samples since aging the samples at 480 °C up to 50 h does not form reverted austenite as reported in previous study [23].

Prior austenite grain size and microstructure analysis

The samples used for the determination of the prior austenite grain size were sanded using SiC paper up to 2500 mesh, washed in distilled water and blow dried followed by polishing using alumina (Al_2O_3) of 1 and 0.05 μm to achieve optical quality of the images. Prior austenite grain size was revealed using an electrolytic etching of 10 V with stepped time. The electrolyte used was 20% chromic acid (H_2CrO_4) solution. The images were taken by Optical Microscopy (MO) using a Zeiss Microscope model Axio Imager M2m. Prior austenite grain size was computed using the software ImageJ following the recommendations of the ASTME112-96 [37]. Martensitic structure

of 18Ni 300 maraging steel was also revealed using a chemical etching with HNO_3 (4%) in methanol by immerging the samples in this reagent up to 10 s by Philips® XL–30 Scanning Electron Microscopy (SEM).

Slow strain rate test (SSRT)

Cylindrical samples manufactured following the ASTM E8/E8M-11 standard [38] were used for SSRT. The produced samples were heat treated as mentioned above (see Section Heat treatments and XRD characterization) in a vacuum sealed quartz tube, air cooled and then categorized as shown in Table 1.

The SSRT was performed in samples in air and in an aqueous solution of 0.6 M NaCl under a simultaneous application of a cathodic potential of −1.2 V_{SCE} [39]. The strain rate of 1.0×10^{-6} s^{-1} was applied for samples tested in air. On the other hand, for the samples tested in an aqueous solution the strain rate used was 1.0×10^{-5} s^{-1} [39]. Prior to each SSRT test all the samples were sanded using SiC paper up to 600 mesh, washed in distilled water and blow dried. A potentiostat/galvanostat (Autolab, Metrohm-EcoChemie) was used to supply the cathodic potential during the SSRT in solution. A three-electrode electrochemical cell was used where the reference electrode was a saturated calomel electrode (SCE) and the counter electrode was a platinum sheet. The working electrode was the samples. Before the SSRT, the samples were immerged in the solution for 30 min in order to determine the open circuit potential (OCP). After reaching the OCP (−0.42 V_{SCE}), the samples underwent cathodic charging for 24 h prior to the SRRT. The tests were performed in a Cortest® machine model Constant's Extension Rate Test with a load cell of 44 kN. All the fractured surfaces after SRRT were observed by SEM. Electron Backscatter Diffraction (EBSD) was also used to analyze the preferred path of the cracks regarding the crystal orientation in the region of crack tip. For this analysis, the fractured region of the samples was prepared by sanding using SiC up to 600 mesh followed by polishing with 6, 3, 1 μm diamond paste and subsequently a final polishing of 0.5 μm colloidal silica suspension. The SSRT were reproduced in duplicate.

Table 1 – Categorized of samples tested on SSRT.

Group	Samples	Annealing	Aging
Group A	S1-480	840 °C/1 h	480 °C/3 h
	S2-480	950 °C/1 h	
	S3-480	1050 °C/1 h	
	S4-480	1150 °C/1 h	
Group B	S1-560	840 °C/1 h	560 °C/1 h
	S2-560	950 °C/1 h	
	S3-560	1050 °C/1 h	
	S4-560	1150 °C/1 h	

Results and discussion

Prior austenite grain size growth

Optical micrographs of 18Ni 300 maraging steel from samples of group A are shown in Fig. 1. It is noticed that the prior

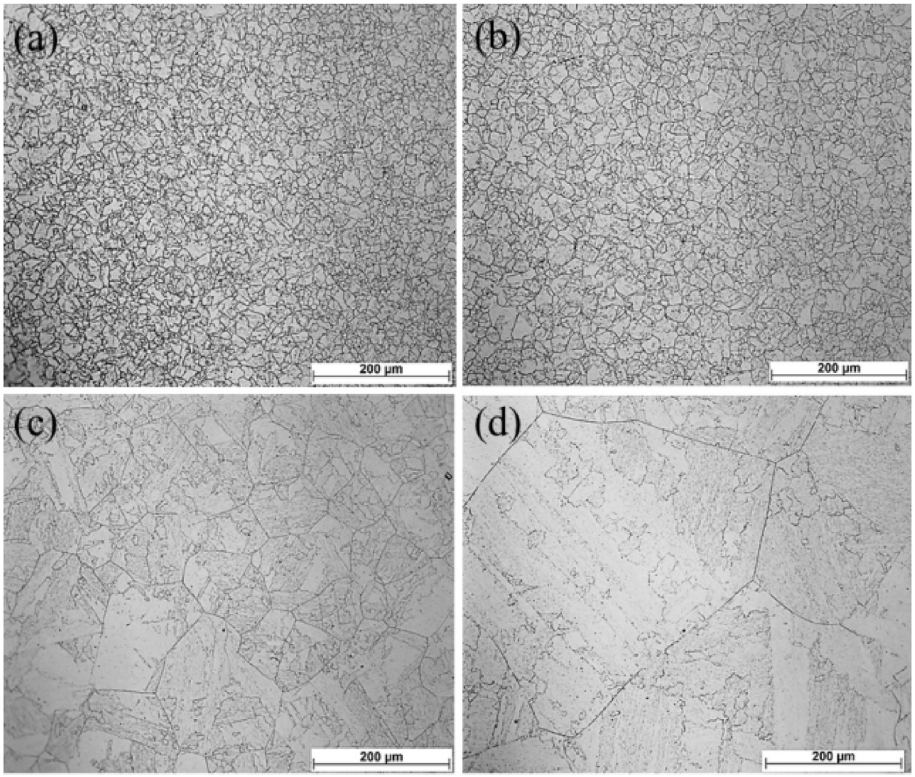

Fig. 1 – Optical micrograph of Co-containing 18Ni 300 maraging steel samples (a) S1-480, (b) S2-480, (c) S3-480 and (d) S4-480.

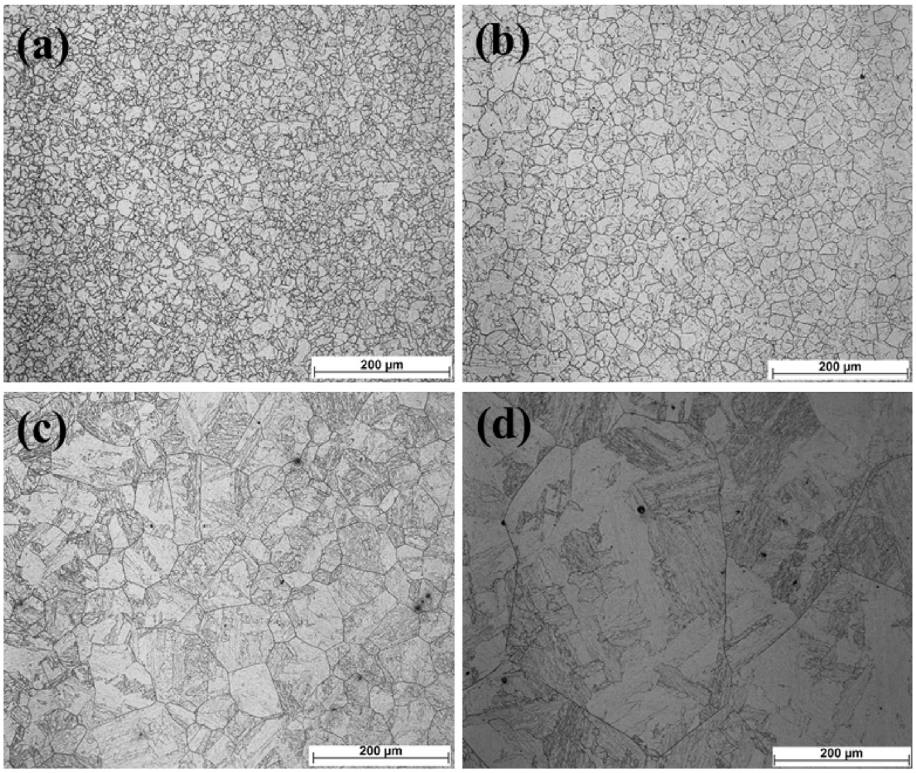

Fig. 2 – Optical micrograph of Co-containing 18Ni 300 maraging steel samples (a) S1-560, (b) S2-560, (c) S3-560 and (d) S4-560.

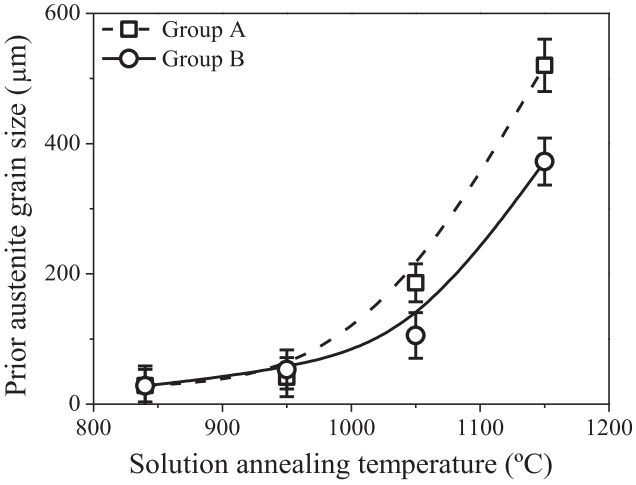

Fig. 3 – Prior austenite grain size of Co-containing 18Ni 300 maraging steel as function of solution annealing temperature.

austenite grain sizeis quiet close forsamples S1-480 and S2-480 around 28 and 48 μm, as can be seen in Fig. 1a and b, respectively. It is known that the grain growth results from grain boundary motion [40], thus, in this condition precipitates that act as barriers preventing the growth of the grain may exist. In addition, in the samples S3-480 and S4-480 was observed a meaningful increase of grain sizes changing to 186 and 520 μm as seen in the optical micrographs displayed in Fig. 1c and d, respectively. Similar results were observed for samples of group B, as seen in Fig. 2. Therefore, it is suggested that solution annealing treatment at temperatures higher than 1000 °C these barriers cease to exist by dissolving the precipitates in the matrix, leaving the dislocations free to move and thus allowing an increase of the prior austenite grains. Grain size average values for both groups as a function of solution annealing temperature is shown in Fig. 3. It is clearly seen that prior austenite grain size followed an exponential tendency growth. Furthermore, in Fig. 4 SEM examination revealed that the microstructure of 18Ni 300 maraging steel in all heat treated conditions were very similar and characteristic of these materials. Fig. 4a and b shows SEM micrographs of samples S4-480 and S4-560, respectively. One can see that the martensitic matrix consisted of well-defined martensite laths.

The quantitative measure of the prior austenite grain size was fixed according to ASTM E 112-96 [37], which ranks the grain on a scale ranging from 00 to 14.0. This classification is called grain size number. Table 2 shows this classification for the average grain size obtained in this research. The maximum grain size corresponds to 00 on this scale. This means that for the solution annealing at 1150 °C for 1 h for both aging conditions, the grain achieved the maximum ASTM value. The heat treatment of aging after the solution annealing did not influence the grain size. These results are in good agreement with results reported by Lima Filho et al., [43].

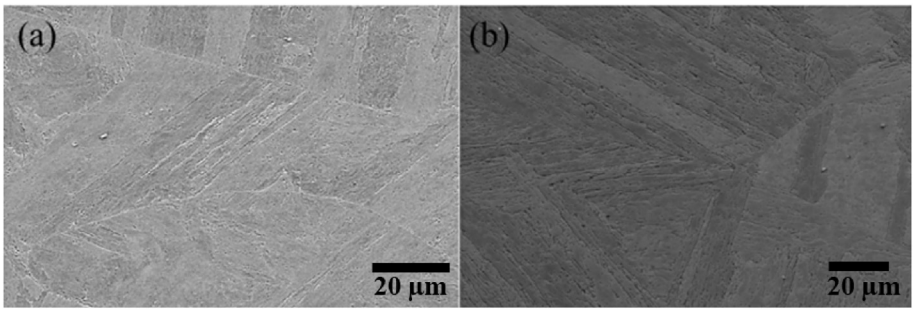

Fig. 4 – SEM micrograph of Co-containing 18Ni 300 maraging steel samples (a) S4-480 and (b) S4-560.

Table 2 – Grain size number classification for the samples solution annealed at several temperatures and aged at 480 °C for 3 h.

ASTM Grain size number	Temperature (°C)	Mean Diameter (μm)
7.5	840	28.6
6.0	950	41.3
2.0	1050	186.2
00	1150	520.2

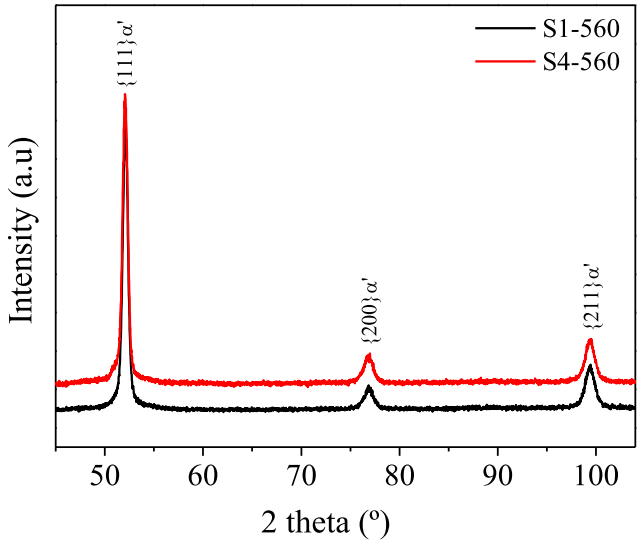

Fig. 5 – XRD pattern of Co-containing 18Ni 300 maraging steel samples (a) S1-560 and (b) S4-560.

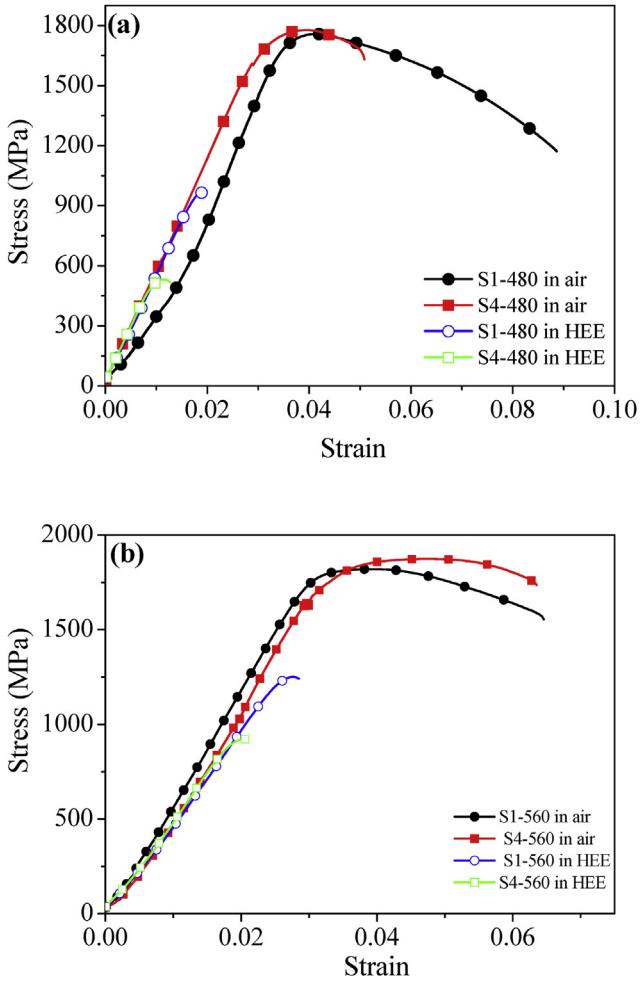

Fig. 6 – (a) SSRT stress–strain curves for samples S1-480 (28.6 μm) and S4-480 (520.2 μm) in air and under dynamic hydrogen charging in 0.6 M NaCl solution and (b) SSRT stress–strain curves for samples S1-560 (28.8 μm) and S4-560 (372.4 μm) in air and under dynamic hydrogen charging in 0.6 M NaCl solution.

XRD analysis

In order to detect the presence of reverted austenite after aging treatment at 560 °C XRD measurement was performed. Fig. 5 shows the XRD patterns for samples S1-560 and S4-560. Only peaks from BBC structure can be seen on this diffractogram corresponding to the martensite phase (α'). It is well-established in literature that aging of 18Ni 300 maraging steel at temperatures above 500 °C for long periods of time can promote formation of reverted austenite as a consequence of the partial dissolution of Ni_3(Ti, Mo) [6–10]. However, in this research, no diffraction peaks corresponding to reverted austenite nor the peaks of the intermetallic compounds were found or the volume fractions of these phases are below the detection limit of technique that is around 5% [41]. Moreover, Sha et al. [6], reported that after aging the 18Ni 300 maraging

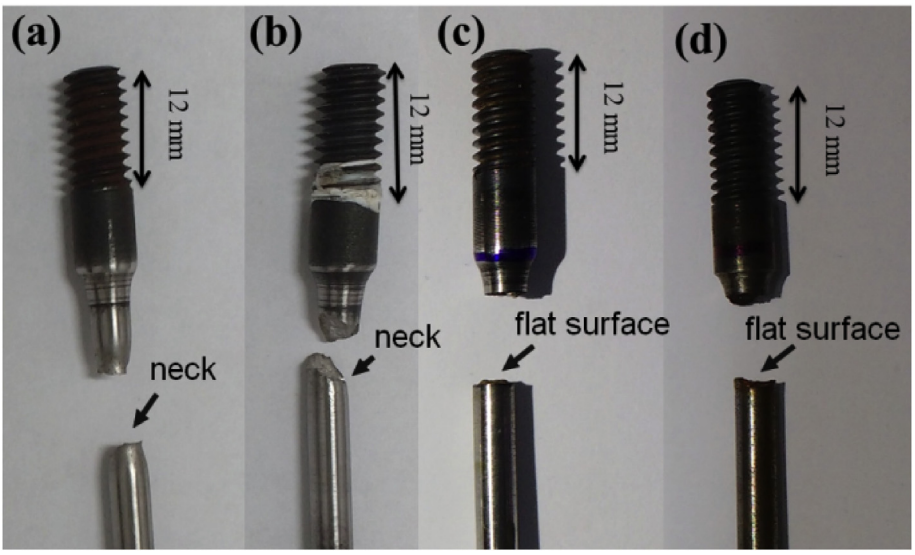

Fig. 7 – Photographic of lateral-view of fractured samples S1-480 and S4-480 tested in air and in HEE.

Table 3 – Mechanical properties taken from SRRT for the samples of 18Ni 300 maraging steel tested in air and in HE.

Sample	UTS in air, MPa	UTS in HEE, MPa	Strain in air, %	Strain in HEE, %	*EI*(Strain), %	*EI*(UTS), %
S1-480	1764	965	8.9	1.9	78.6	45.3
S4-480	1786	527	5.1	1.3	74.5	70.5
S1-560	1825	1243	6.4	2.8	56.2	31.2
S4-560	1873	929	6.3	2.0	68.2	50.4

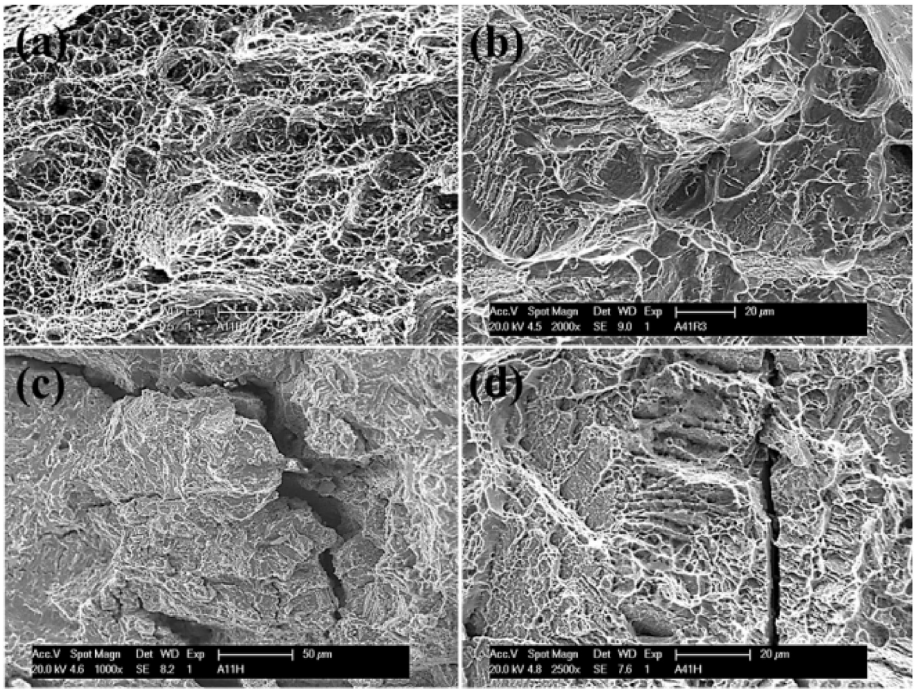

Fig. 8 – SEM fractographs of samples (a) S1-480 in air, (b) S4-480 in air, (c) S1-480 in HEE and (d) S4-480 in HEE.

steel at 510 °C for 128 h the volume fraction of precipitates were less than 4 wt percent. Besides, Pardal et al., observed that the amount of reverted austenite in 18Ni maraging steel aged at 560 °C for 1 h is around 5%. Therefore, reverted austenite may exist in samples S1-560 but it is too low to be detected by XRD.

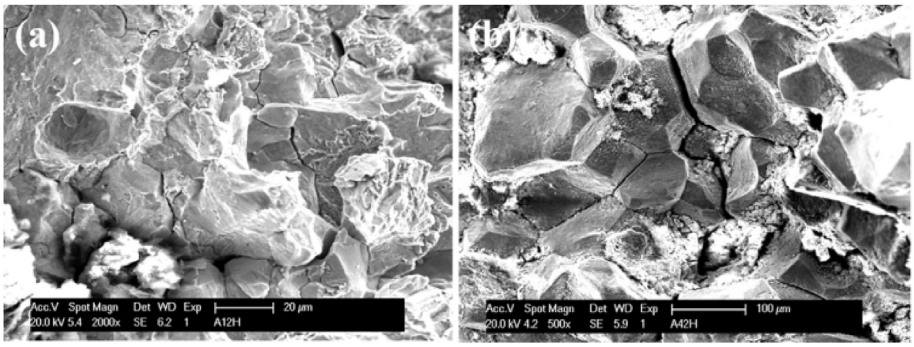

Fig. 9 – SEM fractographs of samples (a) S1-560 and (b) S4-560 in HEE.

Hydrogen embrittlement susceptibility by SRRT

In this section, the results of SSRT are presented for both samples of the 18Ni 300 maraging steel tested in air (inert medium) and tested in aqueous solution of 0.6 M NaCl under simultaneous cathodic polarization of −1.2 V_{ECS}, herein called as hydrogen environment embrittlement (HEE).

Fig. 6a shows the SSRT stress-strain curves of samples S1-480 and S4-480tested in air and in HEE. These conditions of solution annealing were chosen taking into account the smallest and largest grain sizes found in this research. The grain sizes number of steel at the corresponding condition can be seen in brackets. The samples tested in air presented a similar mechanical behavior, thereby, ultimate tensile strength (UTS) for sample S1-480 was around 1764 MPa, while for sample S4-480 an average value of 1786 MPa, however, the sample S1-480 presented a higher elongation than the sample S4-480. On the other hand, the samples tested in HEE presented a drastic reduction of mechanical properties in comparison with the ones tested in air, Fig. 6a. Thus, the samples S1-480 and S4-480 underwent a reduction to 965 and 527 MPa, respectively in their UTS values. Additionally, the steel suffered little or almost no plastic deformation prevailing the fragile fracture. Fig. 7 shows a photographic of lateral-view of fractured samples S1-480 and S4-480 tested in air and in HEE. Fig. 7a–b, tested in air, indicate that the samples exhibited extensive plastic deformation with a neck formation surrounded by a shear lip which is typical of ductile fracture. In contrast, in the samples tested in HEE (Fig. 7c–d) a flat surface without necking was observed confirming the brittle fracture behavior, as seen in Fig. 7a–b. The SSRT stress-strain curves of samples S1-560 and S4-560 tested in air and in HEE are shown in Fig. 6b. These samples exhibited similar mechanical behavior of those found in samples S1-480 and S4-480, Fig. 6a. For tests conducted in air, the samples S1-560 and S4-560 showed a ductile performance with the UTS of 1825 and 1873 MPa, respectively, whereas, for tests performed in HEE, the UTS of these samples presented a reduction to 1243 and 929 MPa. In order to evaluate the HE damage, an embrittlement index (EI) taking into account of the mechanical properties of material was introduced by the following expression [36]:

$$EI(X) = \frac{X_{air} - X_{HE}}{X_{air}} \quad (1)$$

where X is the property under investigation, in this case, the relative UTS and strain reduction. The increase of this index indicates that the mechanical property is more sensible to hydrogen damage. The mechanical properties of S1-480, S4-480, S1-560 and S4-560 obtained from SSRT stress-strain

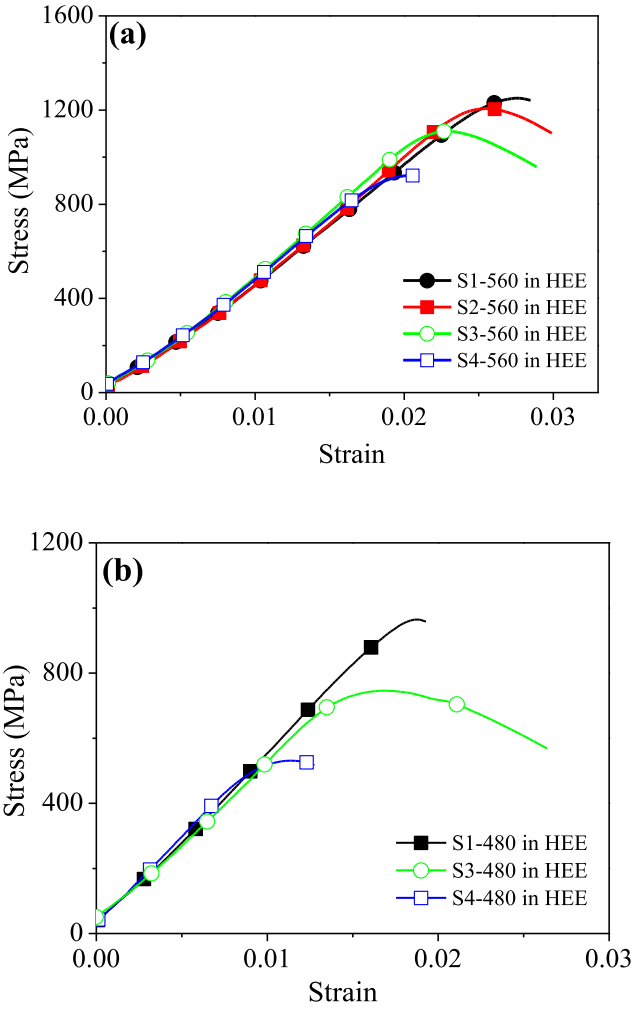

Fig. 10 – SSRT stress–strain curves for samples (a) S1-560 (28.8 μm), S2-560 (53.1 μm), S3-560 (105.3 μm) and S4-560 (372.4 μm) (b) S1-480 (28.6 μm), S3-480 (186.2 μm) and S4-480 (520.2 μm) under dynamic hydrogen charging in 0.6 M NaCl solution.

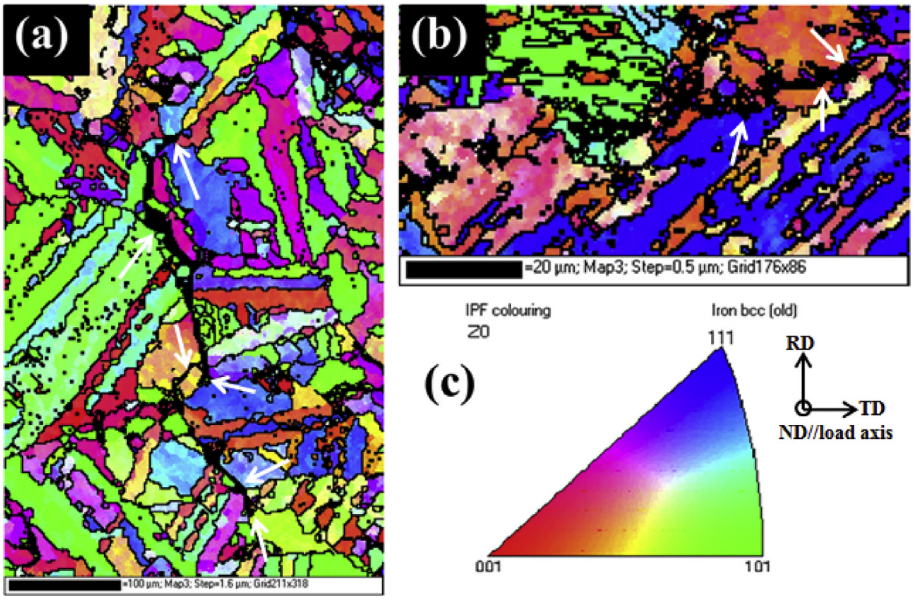

Fig. 11 – EBSD orientation map from the sample (a) S4-560, (b) S1-480 and (c) corresponding standard IPF color triangle.

curves (Fig. 6a–b) are shown in Table 3, as well as, their *EI*. This index indicates that the samples solution annealed at higher temperature are more susceptible to HE in both aging conditions. In addition, the samples aged at 560 °C for 1 h were less susceptible to HE than the ones aged at 480 °C for 3 h. Thereby, suggesting the presence of reverted austenite and/or other precipitates in these samples at this condition. It was reported that maraging steel contenting reverted austenite exhibited the best resistance to HE [23,36].

Furthermore, Fig. 8 shows a SEM view of the fractured surfaces of the samples obtained from SRRT stress-strain curves shown in Fig. 6. In Fig. 8a–b is possible to see the fractograph of samples S1-480 and S4-480, respectively, tested in air. These figures present a great amount of dimples which characterized an extensive plastic deformation before the fracture of steel. Moreover, similar fractographs were obtained from samples S1-560 and S4-560 tested in air and the results were also typical of ductile fracture. SEM micrographs of S1-480 and S4-480 tested in HEE revealed a few dimples, quasi-cleavage regions with the presence of hydrogen-induced cracks propagated into fractured surface, indicating that the material suffered a minimum of plastic deformation before fracture, as can be observed in Fig. 8c–d. Moreover, SEM of fractured surface of samples S1-560 and S4-560 tested in HEE exhibited quasi-cleavage regions characteristic of brittle fracture with hydrogen-assisted intergranular cracks, as seen in Fig. 9a–b. Wang et al. [36], demonstrated that hydrogen-induced cracks propagating along the grain boundaries are a resulting of hydrogen concentration in this regions.

SSRT stress-strain curves for samples S1-560, S2-560, S3-560, and S4-560 are shown in Fig. 10a, while the curves for samples S1-480, S3-480 and S4-480 in Fig. 10b. There is no considerable change in the elastic regime regardless the solution annealing temperature in both aging conditions. Furthermore, one can see that the UTS decreases as the prior austenite grain size of steel increases. It suggested that there may be a relationship between the prior austenite grain size and HE susceptibility. According to Park et al. [42], fine-grained showed superior HE resistance when compared with coarse-grained in API 2 W grade 60 steel. Additionally, Takasawa et al. [35], studied HE of high-strength low-alloy steels and observed that the grain refinement and a reduction in dislocation density are effective in reducing the susceptibility to embrittlement of material.

EBSD maps on the region around the crack propagating on the fracture surface of sample S4-560 and S1-480 are showed in Fig. 11a and b, respectively. The image refers to the crystal orientation in the region of the cracks tips. In this kind of EBSD examination (Fig. 11a–b) the cracks are seen in the map as thicker black lines corresponding the region where no indexing were possible. Additionally, due to the great deformation induced by the fracture of samples, same regions around the crack path were difficult to record a good indexing pattern, thus same black points can be seen as inside the grains. As can be seen in Fig. 11a–b, the cracks initially propagated along red grains, which are orientated through {001} planes parallel to normal direction (//ND), regardless the aging condition. Its known that cleavage fracture occurs preferentially through these crystallographic planes in bcc crystals [43]. Moreover, EBSD also revealed that the crack continued to propagate intergranulary avoiding the grain {101} and {111}//ND, seen in green and blue color in Fig. 11a–b and therefore, passing along their grain boundaries, as indicated by white arrows. These orientations have high crack propagation resistance due to their higher planar density. Previous worked reported that in 18Ni (300) maraging steel the {001} planes can accumulate approximately four times larger strains than {111} planes [24]. Thereby, it can be concluded that the grain orientated to {001}//ND were more prone to hydrogen induced cracks to propagate, due this family's lower planar atomic density, meaning more free sites for the crack propagation, on the

other hand, the denser crystallographic planes {101} and {111} showed higher resistance to hydrogen assisted cracks. These results are in good agreement with other authors [23,36].

Conclusions

The effect of prior austenite grain size of Co-containing 18Ni 300 maraging steel was investigated. Based on the achieved results, the following conclusions can be drawn:

1. The prior austenite grain size was a function of the solution annealing temperature and regardless of the aging temperature.
2. Co-containing 18Ni 300 maraging steel was susceptible to HE at all heat treatment conditions studied. However, samples with smallest prior austenite grains sizes were less susceptible to HE. The prior austenite grain refining improves the HE resistance of material.
3. The cracks for the samples tested in HE propagated along the grain boundaries causing great damage on the fractured surface. The paths for intergranular hydrogen induced crack propagation were in grain orientated along to {001}//ND, while the other orientations {110} and {111}// ND were more resistant to crack propagation.

Acknowledgment

The present work was carried out with the support of CNPq, National Council of Scientific and Technological Development - Brazil (grant number 309160/2016-2). The authors would also like to acknowledge the Federal Fluminense University in Brazil where the SRRT measurements were carried out. Luis P. M. Santos thanks CNPq for their scholarship 141746/2015-7. This research was financed in part by the Coordenação de Aperfeiçoamento de Pessoal de Nível Superior - Brasil (CAPES) - Finance Code 001. Finally the authors would like to thank the Central Analítica-UFC/CT-INFRA/MCTI-SISANO/Pró-Equipamentos CAPES for the support.

REFERENCES

[1] Magnée A, Drapier JM, Dumont J, Coutsouradis D, Habraken L. Cobalt-containing high-strength steels. Brussels: Centre d'Information du Cobalt; 1974.
[2] Sha W, Guo Z. Maraging steels. Cambrigde: Woodhead Publishing Limited New Cambridge; 2009.
[3] Floreen S. The physical metallurgy of maraging steels. Metall Rev 1968;13:115–28.
[4] Floreen S, Decker RF. Heat treatment of 18% Ni maraging steel. Trans. ASM. 1962;55:518–30.
[5] Vasudevan VK, Kim SJ, Wayman CM. Precipitation reactions and strengthening behavior in 18 wt pct nickel maraging steels. Metall Trans A 1990;21:2655–68. https://doi.org/10.1007/BF02646061.
[6] Sha W, Cerezo A, Smith GDW. Phase chemistry and precipitation reactions in maraging steels: Part I. Introduction and study of Co-containing C-300 steel. Metall Mater Trans A 1993;24:1221–32.
[7] Viswanathan UK, Dey GK, Asundi MK. Precipitation hardening in 350 grade maraging steel. Metall Trans A 1993;24:2429–42. https://doi.org/10.1007/BF02646522.
[8] Tewari R, Mazumder S, Batra IS, Dey GK, Banerjee S. Precipitation in 18 wt% Ni maraging steel of grade 350. Acta Mater 2000;48:1187–200.
[9] Li X, Yin Z. Reverted austenite during aging in 18Ni (350) maraging steel. Mater Lett 1995;24:239–42.
[10] Viswanathan UK, Dey GK, Sethumadhavan V. Effects of austenite reversion during overageing on the mechanical properties of 18 Ni (350) maraging steel. Mater Sci Eng A 2005;398:367–72. https://doi.org/10.1016/j.msea.2005.03.074.
[11] Ahmed M, Ali A, Hasnain SK, Hashmi FH, Khan AQ. Magnetic properties of maraging steel in relation to deformation and structural phase transformations. Acta Metall Mater 1994;42:631–8.
[12] Tavares SSM, Abreu HFG, Neto JM, Da Silva MR, Popa I. A thermomagnetic study of the martensite–austenite phase transition in the maraging 350 steel. J Alloy Compd 2003;358:152–6.
[13] Nageswara Rao M, Mohan MK, Uma Maheswara Reddy P. Environmentally assisted cracking of 18%Ni maraging steel. Corros Sci 2009;51:1645–50. https://doi.org/10.1016/j.corsci.2009.04.011.
[14] Tsay LW, Lu HL, Chen C. The effect of grain size and aging on hydrogen embrittlement of a maraging steel. Corros Sci 2008;50:2506–11.
[15] Zhang YP, Shi DM, Chu WY, Qiao LJ, Shi YL, Zheng SL, Wang SB. Hydrogen-assisted cracking of T-250 maraging steel. Mater Sci Eng A 2007;471:34–7.
[16] Tsay LW, Chi MY, Wu YF, Wu JK, Lin D-Y. Hydrogen embrittlement susceptibility and permeability of two ultra-high strength steels. Corros Sci 2006;48:1926–38. https://doi.org/10.1016/j.corsci.2005.05.042.
[17] Tsay LW, Hu YF, Chen C. Embrittlement of T-200 maraging steel in a hydrogen sulfide solution. Corros Sci 2005;47:965–76.
[18] Wu CP, Tsay LW, Chen C. Notched tensile testing of T-200 maraging steel and its laser welds in hydrogen. Mater Sci Eng A 2003;346:302–9. https://doi.org/10.1016/S0921-5093(02)00552-X.
[19] Pao PS, Wei RP. Hydrogen assisted crack growth in 18Ni (300) maraging steel. Scripta Metall 1977;11:515–20.
[20] Gangloff RP, Wei RP. Gaseous hydrogen assisted crack growth in 18 nickel maraging steels. Scripta Metall 1974;8:661–7.
[21] Hudak SJ, Wei RP. Hydrogen enhanced crack growth in 18 Ni maraging steels. Metall. Trans. A. 1976;7:235–41.
[22] Reddy KG, Arumugam S, Lakshmanan TS. Hydrogen embrittlement of maraging steel. J Mater Sci 1992;27:5159–62.
[23] Santos LPM, Béreš M, Bastos IN, Tavares SSMM, Abreu HFGG, Gomes da Silva MJ, da Silva MJG. Hydrogen embrittlement of ultra high strength 300 grade maraging steel. Corros Sci 2015;101:12–8. https://doi.org/10.1016/j.corsci.2015.06.022.
[24] Béreš M, Wu L, Santos LPM, Masoumi M, da Rocha Filho FAM, da Silva CC, de Abreu HFG, da Silva MJG. Role of lattice strain and texture in hydrogen embrittlement of 18Ni (300) maraging steel. Int J Hydrogen Energy 2017;42:14786–93.
[25] Dwivedi SK, Vishwakarma M. Hydrogen embrittlement in different materials: a review. Int J Hydrogen Energy 2018;43:21603–16. https://doi.org/10.1016/j.ijhydene.2018.09.201.
[26] Boukortt H, Amara M, Meliani MH, Bouledroua O, Muthanna BGN, Suleiman RK, Sorour AA, Pluvinage G. Hydrogen embrittlement effect on the structural integrity of

API 5L X52 steel pipeline. Int J Hydrogen Energy 2018;43:19615–24. https://doi.org/10.1016/j.ijhydene.2018.08.149.
[27] Koyama M, Akiyama E, Lee Y-K, Raabe D, Tsuzaki K. Overview of hydrogen embrittlement in high-Mn steels. Int J Hydrogen Energy 2017;42:12706–23. https://doi.org/10.1016/j.ijhydene.2017.02.214.
[28] Stenerud G, Wenner S, Olsen JS, Johnsen R. Effect of different microstructural features on the hydrogen embrittlement susceptibility of alloy 718. Int J Hydrogen Energy 2018;43:6765–76. https://doi.org/10.1016/j.ijhydene.2018.02.088.
[29] Li S, Chen C, Liu Y, Yu H, Wang X. Influence of surface martensite layer on hydrogen embrittlement of Fe-Mn-C-Mo steels in wet H2S environment. Int J Hydrogen Energy 2018;43:16728–36. https://doi.org/10.1016/j.ijhydene.2018.06.011.
[30] Örnek C, Reccagni P, Kivisäkk U, Bettini E, Engelberg DL, Pan J. Hydrogen embrittlement of super duplex stainless steel–Towards understanding the effects of microstructure and strain. Int J Hydrogen Energy 2018;43:12543–55. https://doi.org/10.1016/j.ijhydene.2018.05.028.
[31] Wang Y, Cheng G, Qin M, Li Q, Zhang Z, Chen K, Li Y, Hu H, Wu W, Zhang J. Effect of high temperature deformation on the microstructure, mechanical properties and hydrogen embrittlement of 2.25 Cr–1Mo-0.25 V steel. Int J Hydrogen Energy 2017;42:24549–59. https://doi.org/10.1016/j.ijhydene.2017.07.237.
[32] Wang Y, Wu X, Li X, Wu W, Gong J. Combined effects of prior plastic deformation and sensitization on hydrogen embrittlement of 304 austenitic stainless steel. Int J Hydrogen Energy 2019;44:7014–31. https://doi.org/10.1016/j.ijhydene.2019.01.122.
[33] Liu Q, Zhou Q, Venezuela J, Zhang M, Atrens A. The role of the microstructure on the influence of hydrogen on some advanced high-strength steels. Mater Sci Eng A 2018;715:370–8.
[34] Shen S, Li X, Zhang P, Nan Y, Yang G, Song X. Effect of solution-treated temperature on hydrogen embrittlement of 17-4 PH stainless steel. Mater Sci Eng A 2017;703:413–21.
[35] Takasawa K, Ikeda R, Ishikawa N, Ishigaki R. Effects of grain size and dislocation density on the susceptibility to high-pressure hydrogen environment embrittlement of high-strength low-alloy steels. Int J Hydrogen Energy 2012;37:2669–75. https://doi.org/10.1016/j.ijhydene.2011.10.099.
[36] Wang G, Yan Y, Li J, Huang J, Qiao L, Volinsky AA. Microstructure effect on hydrogen-induced cracking in TM210 maraging steel. Mater Sci Eng A 2013;586:142–8.
[37] American Society for testing and materials (filadelfia Pennysylvania). ASTM E112-96 (2004) e2: Standard Test Methods for Determining Average Grain Size. ASTM; 2004.
[38] A.H. Standard, ASTM E8/E8M-11, Standard test method for Tension Testing of Metallic Materials, Google Sch. (n.d.).
[39] Standard G129-00. Standard practice for slow strain rate testing to evaluate the susceptibility of metallic materials to environmentally assisted cracking. American Society for Testing and Materials; 2000.
[40] Wakai F, Yoshida M, Shinoda Y, Akatsu T. Coarsening and grain growth in sintering of two particles of different sizes. Acta Mater 2005;53:1361–71.
[41] Cullity B. Elements of diffraction. 2nd ed. Addison-Wesley Publishing Company, Inc.; 1978.
[42] Park C, Kang N, Liu S. Effect of grain size on the resistance to hydrogen embrittlement of API 2W Grade 60 steels using in situ slow-strain-rate testing. Corros Sci 2017;128:33–41.
[43] Pineau A, Benzerga AA, Pardoen T. Failure of metals I: brittle and ductile fracture. Acta Mater 2016;107:424–83.